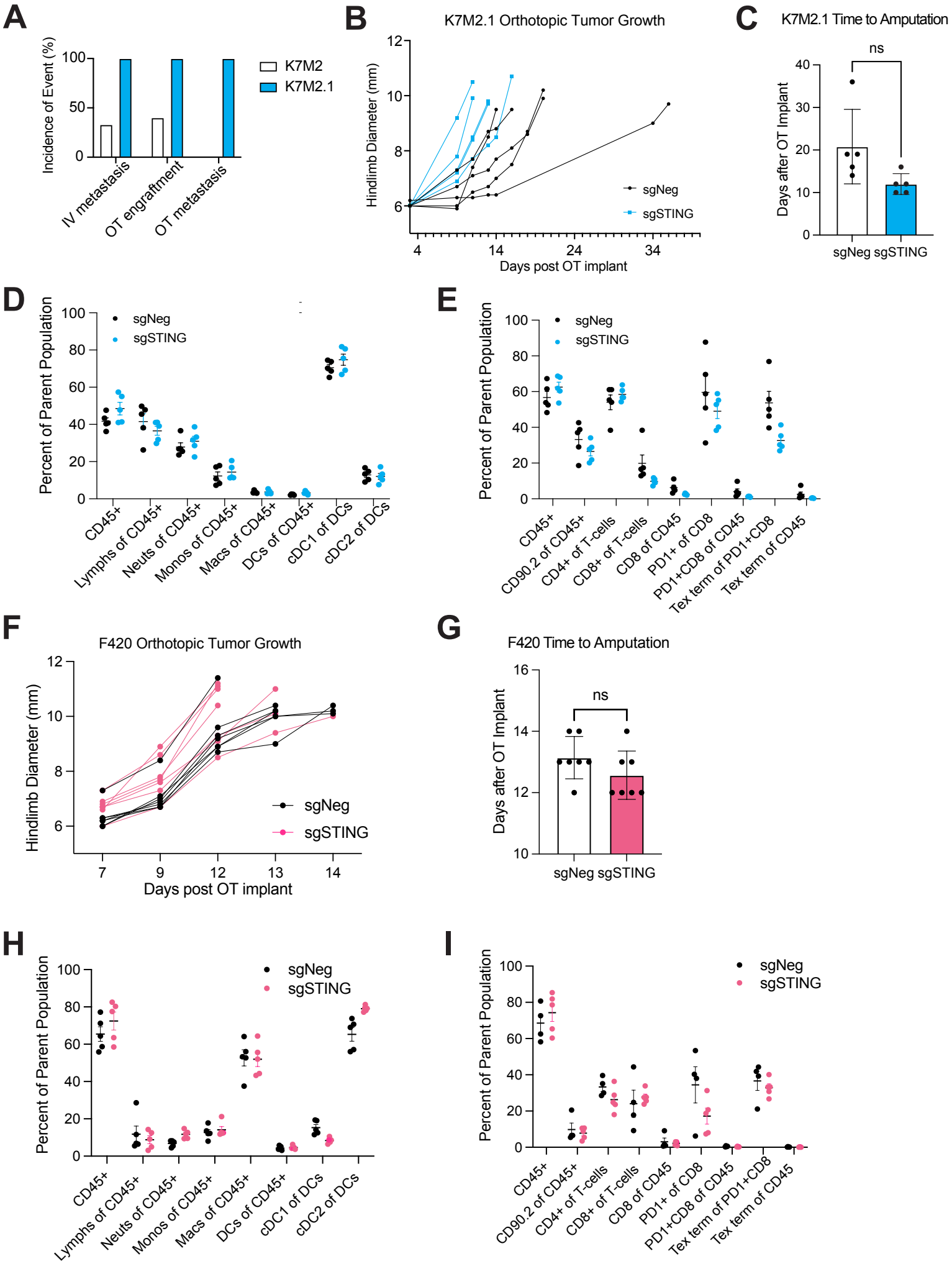

A
Incidence of Event (%)
100
50
0
K7M2
K7M2.1
IV metastasis
OT engraftment
OT metastasis
B
K7M2.1 Orthotopic Tumor Growth
Hindlimb Diameter (mm)
12
10
8
6
sgNeg
sgSTING
4
14
24
34
Days post OT implant
C
K7M2.1 Time to Amputation
ns
Days after OT Implant
40
30
20
10
0
sgNeg sgSTING
D
Percent of Parent Population
100
80
60
40
20
0
sgNeg
sgSTING
CD45+
Lymphs of CD45+
Neuts of CD45+
Monos of CD45+
Macs of CD45+
DCs of CD45+
cDC1 of DCs
cDC2 of DCs
E
Percent of Parent Population
sgNeg
sgSTING
CD45+
CD90.2 of CD45+
CD4+ of T-cells
CD8+ of T-cells
CD8 of CD45
PD1+ of CD8
PD1+CD8 of CD45
Tex term of PD1+CD8
Tex term of CD45
F
F420 Orthotopic Tumor Growth
Hindlimb Diameter (mm)
12
10
8
6
sgNeg
sgSTING
7
9
12
13
14
Days post OT implant
G
F420 Time to Amputation
Days after OT Implant
16
14
12
10
ns
sgNeg sgSTING
H
Percent of Parent Population
100
80
60
40
20
0
sgNeg
sgSTING
CD45+
Lymphs of CD45+
Neuts of CD45+
Monos of CD45+
Macs of CD45+
DCs of CD45+
cDC1 of DCs
cDC2 of DCs
I
Percent of Parent Population
sgNeg
sgSTING
CD45+
CD90.2 of CD45+
CD4+ of T-cells
CD8+ of T-cells
CD8 of CD45
PD1+ of CD8
PD1+CD8 of CD45
Tex term of PD1+CD8
Tex term of CD45

Figure S1. S1A. In vivo behavior of parental K7M2 vs. derived line K7M2.1. IV studies with K7M2 (n=6) reached a 4-6 wk endpoint; K7M2.1 mice (n=4) endpoint 3 wks. OT studies monitored for 10-18 wks, with a metastatic endpoint of 6-8 wks post-amputation; K7M2 (n=5), K7M2.1 (n=3). S1B-C. Primary tumor growth for K7M2.1 sgNeg (n=5) vs. sgSTING (n=5); S1D-E. Immune infiltration by flow cytometry (left, myeloid panel; right, lymphoid panel in OT osteosarcoma tumors, K7M2.1 sgNeg (n=5) and sgSTING (n=5). S1F-G. Murine osteosarcoma cell line F420 sgNeg (n=7) and sgSTING (n=7) primary tumor growth. S1H-1. Immune infiltration by flow cytometry (left, myeloid panel; right, lymphoid panel in OT osteosarcoma tumors, F420 sgNeg (n=4-5) and sgSTING (n=5). Data are shown as mean (A), mean ± SD (C, G); significant differences were not observed; unpaired t test (C, G); unpaired t test followed by two-stage step-up multiple comparisons (D, E, H, I).

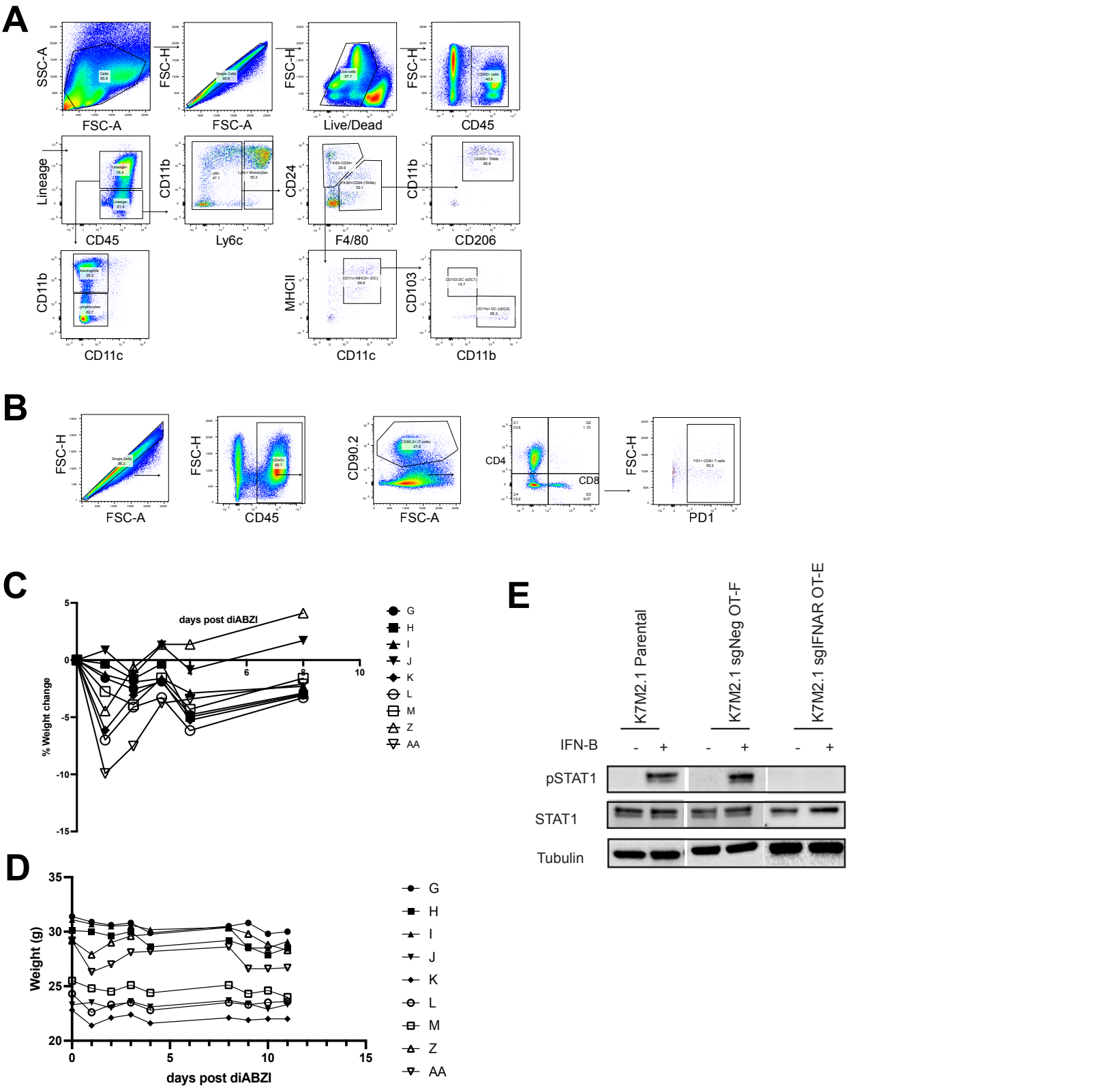


Figure S2. S2A-B. Immunophenotyping of murine osteosarcoma tumors (adapted from ref. 24). Fresh or viably frozen OT tumors were digested and partitioned for myeloid (S2A) and T lymphoid (S2B) panels. S2A. Myeloid markers within lineage (CD90.2, CD45R/B220, Ly-6G, NK-1.1, Siglec-F) negative population, including CD11b, Ly6c, CD24, F4/80, CD206, MHCII, CD11c, and CD103. Neutrophils were gated as shown by identifying the CD11b+ cells in the Lin+ gate (which included Ly-6G), except for the 0h vs. 2h timepoint in Fig. 3C-D wherein Ly-6G was moved out of Lin+ and gated after CD45. For flow cytometry of BALB/c-derived tumors, NK cells were not included in Lin+ and where specified a distinct NK marker (CD49b) was utilized to characterize NK cell changes. S2B. T lymphoid markers within CD90.2 positive gate, including CD4, CD8, CD25, and PD1. S2C-D. Systemic diABZI treatment is well tolerated. Body weight, expressed as percent change from baseline (S2C) in K7M2.1 orthotopic tumor-bearing mice treated with diABZI (n=9) through day 8 post-treatment, with similar short-term toxicity observed after repeat dosing (S2D) and responding to supportive care as described in the Methods. Data shown for individual animals. S2E. Western blot validation of K7M2.1 sgNeg and sgIFNAR cell lines generated as described in Methods (pooled single cell clones passaged through OT tumor.

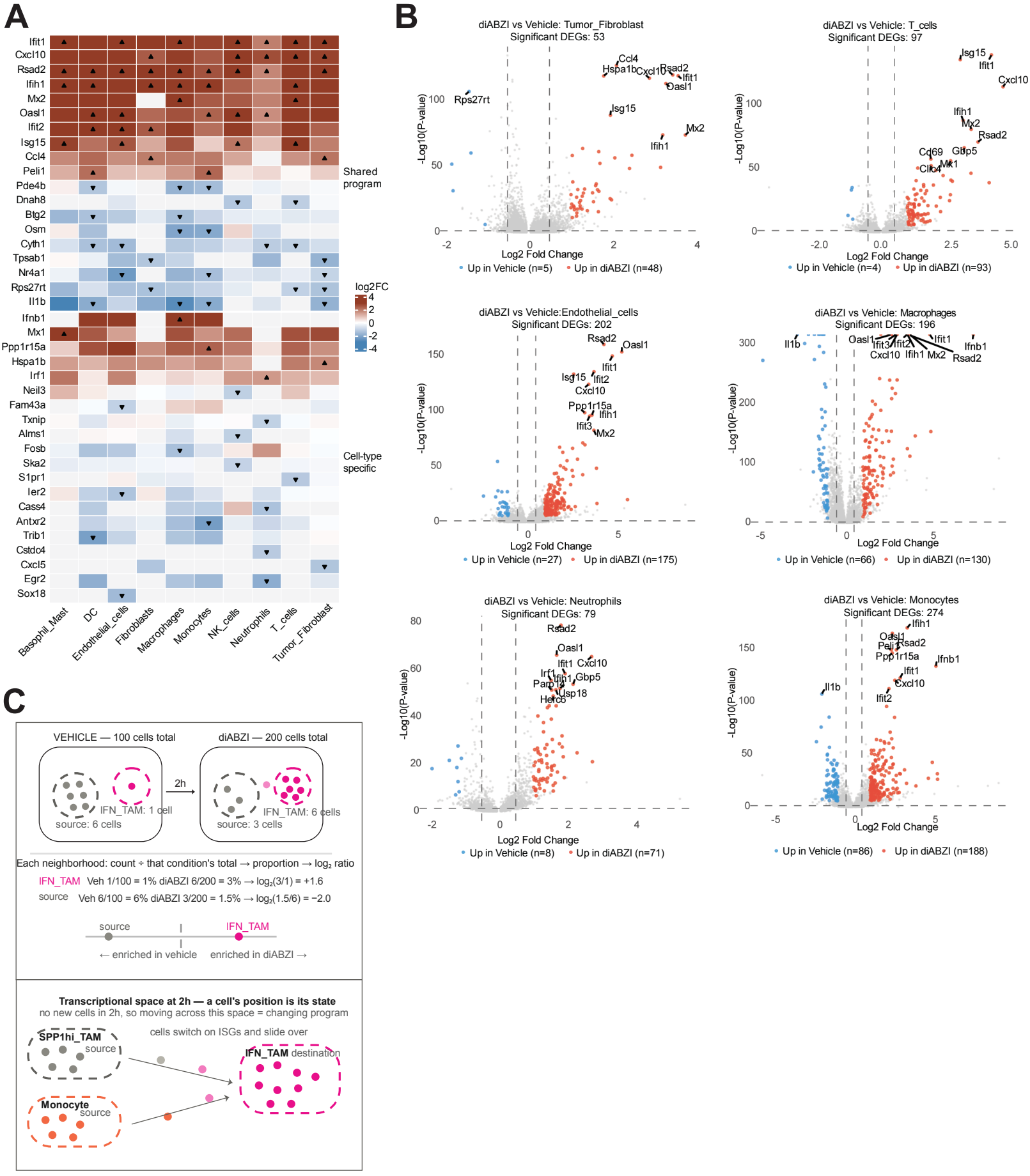


Fig. S3. S3A. Top 5 diABZI-induced and -repressed genes across all TME cell types, sorted by shared programs with at least 1 shared top-5 up/down DEG (top) and cell type specific top-5 up/down DEGs (bottom). S3B. Volcano plots showing DEGs per cell type in response to diABZI. S3C. Schematic of Milo differential abundance analysis and proposed interpretation (ref 29), generated by AI (Claude, Anthropic).

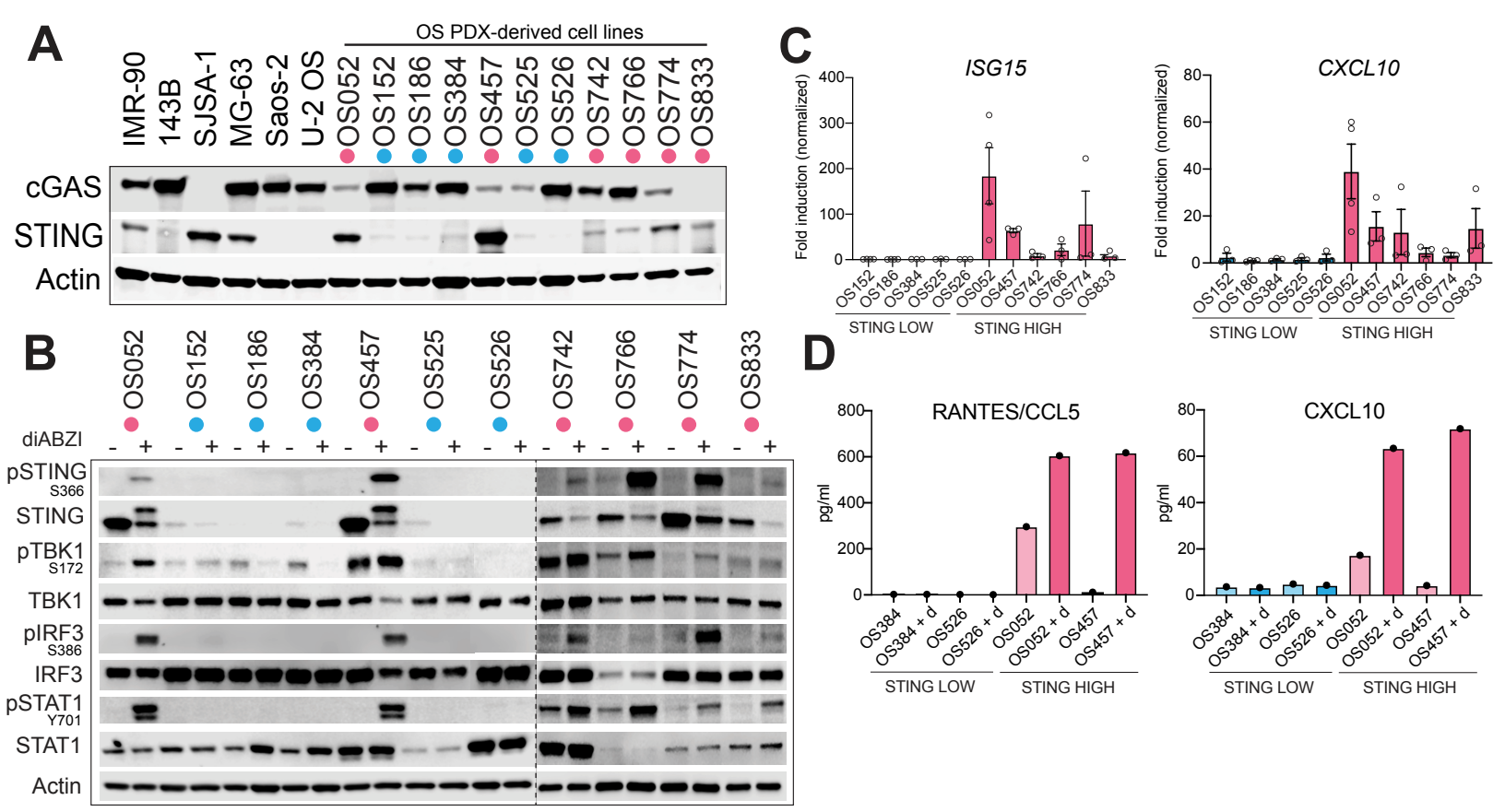


Fig. S4. S4A. Immunoblot for cGAS and STING in osteosarcoma cell lines under standard culture conditions. S4B. STING effector activity in osteosarcoma PDX cell lines 6h after STING agonist (diABZI). S4C. RT-qPCR of interferon stimulated genes in osteosarcoma PDX cell lines 24h after diABZI stimulation (mean ± SEM; n=3-4 independent experiments). S4D. Pro-inflammatory cytokine levels (pg/mL) in conditioned media of STING-high (OS052, OS457) vs. -low (OS384, OS526) osteosarcoma PDX cell lines upon stimulation with diABZI ("+ d") for 6h (mean; n=2). Cell lines with high vs. low STING protein in S4A are color coded accordingly as STING-high (pink) or STING-low (blue).

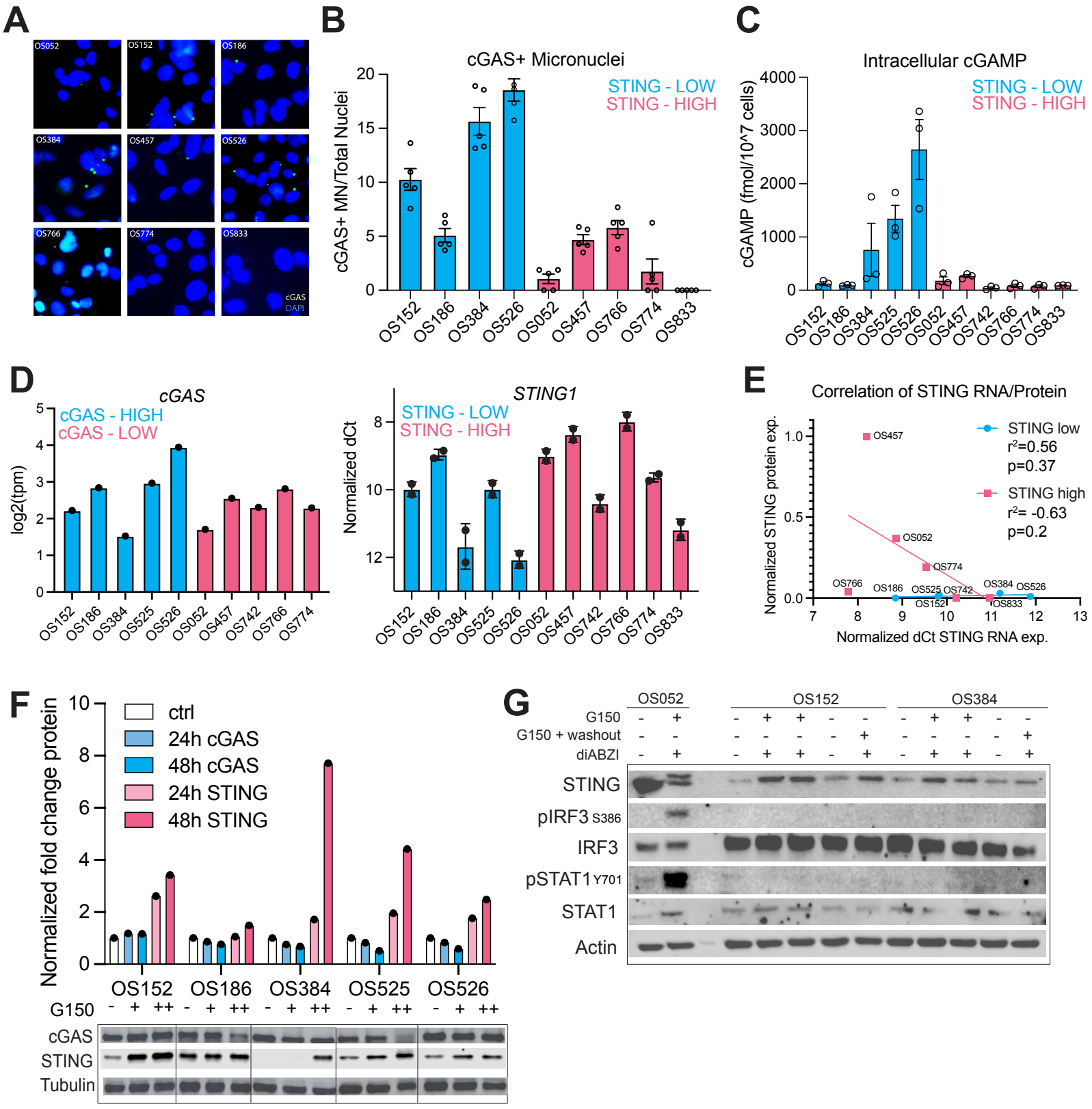


Figure S5. S5A-B. Micronuclei (MN) are identified in all osteosarcoma cell lines but vary in overall burden and cGAS recruitment to MN. (A) Representative IF images demonstrating MN (DAPI) and cGAS (FITC) across osteosarcoma PDX cell line panel. (B) Manual quantification of percentage of MN with co-positivity for cGAS of total nuclei (mean ± SEM; n=5 FOV/cell line). S5C. Intracellular cGAMP as measured by ELISA across panel of osteosarcoma PDX cell lines (mean ± SEM; n=3 per cell line across 3 independent experiments). S5D. CGAS transcript analysis by bulk RNAseq and STING1 transcript analysis by qPCR in osteosarcoma PDX cell lines. S5E. Spearman correlation of STING1 RNA expression by qPCR (Fig. S5D) and protein expression quantified (Fig. S4A) for STING-low/high groups separately. S5F. Treatment of STING-low PDX cell lines with cGAS inhibitor increases total STING protein levels. S5G. Immunoblot analysis for STING activation after combination treatment with cGAS inhibitor (± washout) and STING agonist (diABZI).

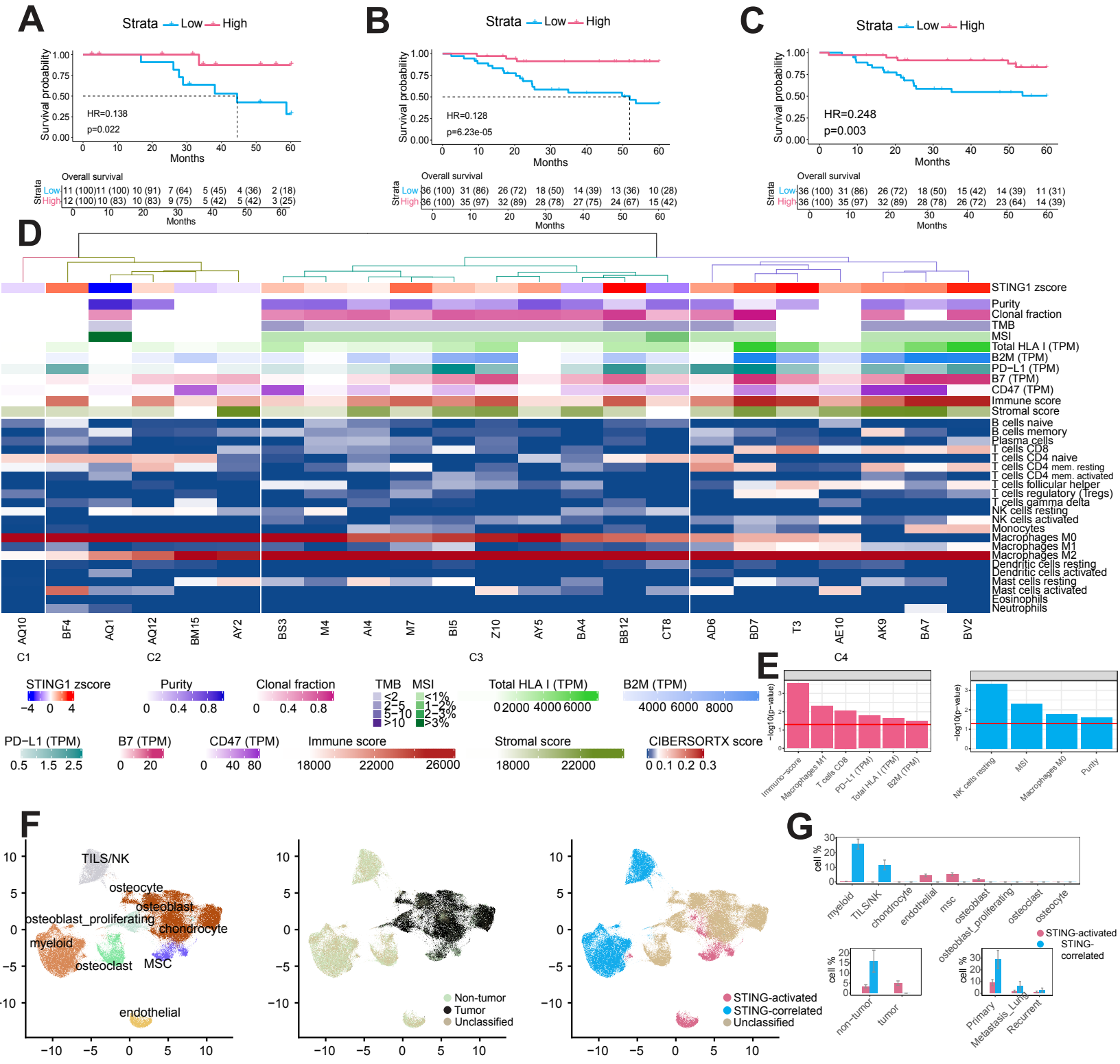


Figure S6. S6A. Overall survival with samples (n=23) stratified by STING-activated enrichment (top vs. bottom 50%), S6B-C. Overall survival validation of prognostic significance of STING-activated (7B) and STING-correlated (7D) in an independent osteosarcoma dataset (n=72). S6D. Immuno-profiling of osteosarcoma diagnostic biopsy tissue samples (n=23) using CIBERSORTX and annotated with genomic features from RNAseq and WGS data. Missing genomic annotations indicate samples where WGS was unavailable. Based on the immune cell type scores, samples were clustered into 4 groups using k-means clustering. S6E. Using a generalized linear model, genomic and immune cell features were analyzed to determine how predictive each feature was to STING-activated signature score (z-scaled) (left plot=positive association; right plot=negative association). Significance scores were calculated for each feature. Multiple testing correction was performed using Benjamini–Hochberg. Features that had a predictive significance (corrected) less than 0.05 are shown. The red line indicates p=0.05. S6F. 11 treated osteosarcomas (9 primary and 2 metastases) in (ref 34) with UMAP rendering of all cells in all samples by cell type (left), tumor vs. normal (middle), and STING signature enrichment (right). S6G. Bar plots indicating percentage of cells in indicated categories by cell type.

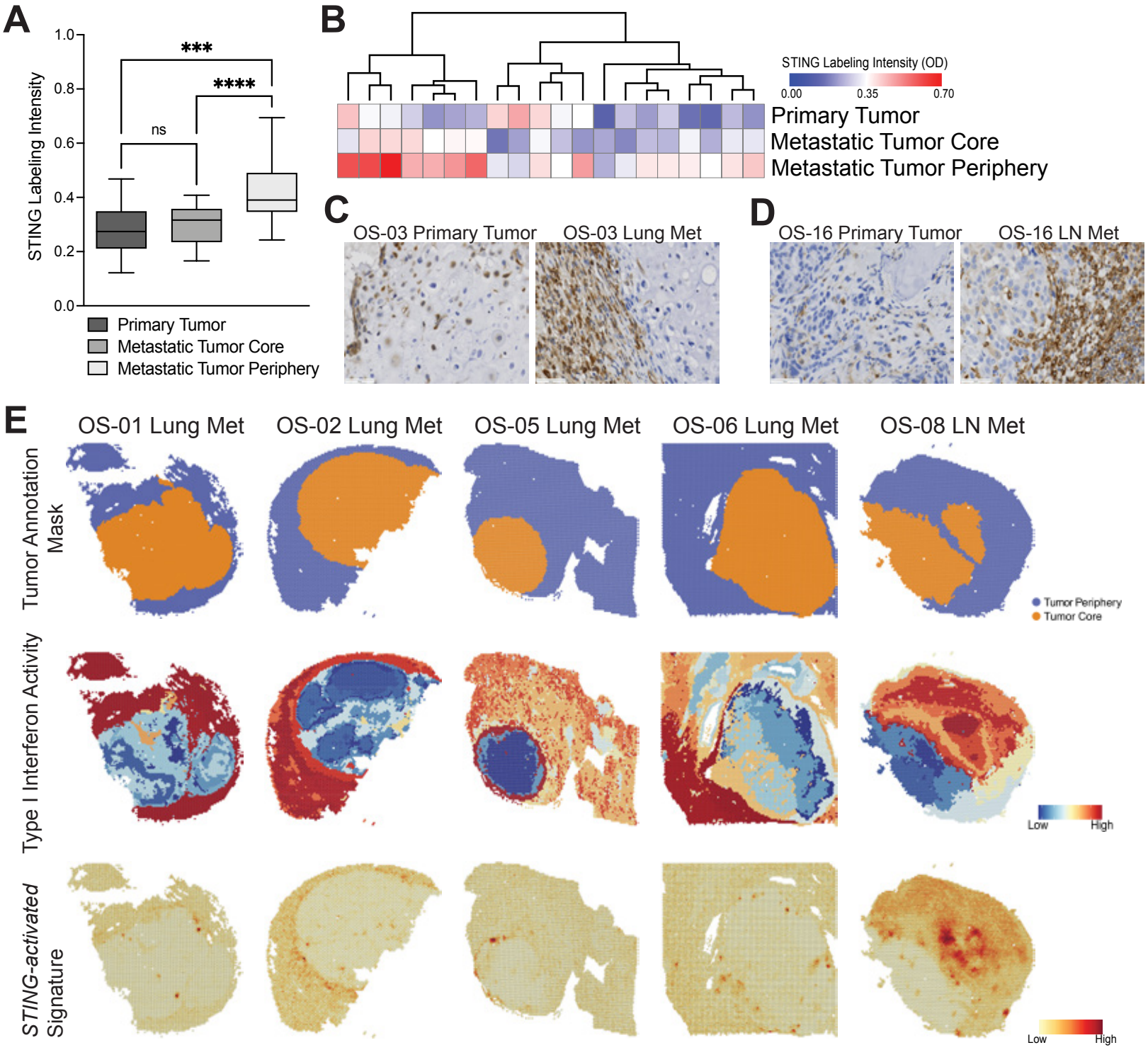


Figure S7. S7A. Boxplot showing STING labeling intensity (avg. OD) in n=20 matched primary-metastatic specimens. Statistical significance ($p<0.05$) determined by repeated measures one-way ANOVA. S7B. Unsupervised hierarchical clustering of STING labeling intensity. S7C-D. Representative images of STING labeling intensity in (C) the primary tumor core (left) and pulmonary metastatic lesion (right) of specimen OS-03 and (D) the primary tumor (left) and lymph node metastatic lesion (right) of osteosarcoma specimen OS-16. Scale bar = 50 um. S7E. Spatial transcriptomic profiling showing regional distribution of type I interferon activity and STING activation signature in metastatic osteosarcoma specimens. Top row: masked spatial plots differentially highlighting tumor core and tumor periphery. Middle row: spatial plots of CytoSig analysis showing the regional distribution and relative strength of type 1 interferon signaling activity. Bottom row: spatial enrichment of STING-activated signature.